Journal of Heat and Mass Transfer Research

Journal homepage: https://jhmtr.semnan.ac.ir

Semnan University

ISSN: 2383-3068

Research Article

Heat Transfer and Thermal Radiation Effects on the Phan-Thien-Tanner Fluid Model Under Peristaltic Flow with a Permeable Porous Wall

Ballekere Ramakrishna Mahalakshmi [a], Mahadev Madivalappa Channakote [a *], Shekar Marudappa [b], Shivkumar Biradar [c]

[a] *Department of Mathematics and Statistics, M.S. Ramaiah University of Applied Sciences, Bengaluru, Karnataka, India*

[b] *Department of Mathematics, B.M.S College of Engineering, Bengaluru*

[c] *Department of Mathematics, Government First grade college, Chitaguppa, Karnataka, India*

ARTICLE INFO

Article history:

Received: 2025-01-05

Revised: 2025-03-18

Accepted: 2025-04-03

Keywords:

PTT fluid;

Peristaltic flow;

Heat transfer;

Thermal radiation;

Permeable wall.

ABSTRACT

Peristalsis is crucial in industrial applications for transporting delicate or corrosive liquids through tubes without direct contact with mechanical elements. It enables precise fluid flow control in pharmaceuticals, food processing, and chemical handling. The current article deals with the combine effects of heat transfer and thermal radiation on peristaltic flow of a Phan-Thien-Tanner (PTT) fluid through channel. The nature of the walls is assumed to be permeable. The theoretical model considers the motion of conductive physiological fluids affected by heat, thermal radiation, and permeability. This model has important biomedical applications such as improving drug delivery systems, optimizing thermal therapies, and analyzing blood flow behavior with external heat sources. The flow is modelled using momentum, and energy, equations with Saffmann boundary conditions at the walls. The governing equations, including the continuity, momentum, and energy equations, are simplified under the low Reynolds number and long wavelength approximations. An analytical approach is used to solve the coupled equations, which gives detailed profiles of velocity, temperature, and pressure fields in the channel. The impact of important parameters like the Weissenberg number, porosity factor, radiation parameter, and Brinkman number on flow characteristics and temperature distribution is thoroughly investigated using Mathematica Software. The study shows that increasing the Weissenberg number results in a more elastic fluid, improving energy storage and redistribution during deformation. Higher values of Darcy number (Da), Prandtl number (Pr), and radiation parameter (Rd) lead to a decrease in temperature profile, indicating the impact of thermal radiation and permeability on flow efficiency and heat transfer regulation. These findings are valuable for optimizing microfluidic devices, biomedical systems, and porous media applications, where precise thermal management and flow control are crucial.

1. Introduction

Peristalsis, a wave-like pattern of muscle contractions, is responsible for moving biological fluids from one place to another through muscular contractions. These contractions originate in the digestive system and are a natural and essential part of its function. The ureter,

* **Corresponding author.**
E-mail address: *mchannakote@rediffmail.com*

Cite this article as:
Mahalakshmi, B. R., Channakote, M. M, Marudappa, S. and Biradar, S., 2026. Heat Transfer and Thermal Radiation Effects on the Phan-Thien-Tanner Fluid Model Under Peristaltic Flow with a Permeable Porous Wall. *Journal of Heat and Mass Transfer Research*, 13(1), pp. 89-100.
https://doi.org/10.22075/JHMTR.2025.36391.1668

which connects the kidney and bladder, also exhibits peristaltic movement. Due to its critical role, peristaltic flow is widely used for both physiological and mechanical purposes in various conditions. Its applications extend to industries such as nuclear, ceramic, porcelain, oil, industrial, paper, and food sectors, where it is utilized daily. The concept of fluid movement through peristaltic transfer was first introduced by Latham [1], and subsequent research by Shapiro et al. [2] laid the groundwork for further studies. Numerous researchers have focused on advancing peristaltic transport by investigating the effects of various physical properties across different media, resulting in promising outcomes. Extensive research has been conducted using both theoretical and experimental approaches, with significant contributions from researchers in this field [3-11].

Recent breakthroughs have enabled significant practical applications for investigating peristaltic transport using Phan-Thien and Tanner (PTT) liquid in various geometrical forms across several sectors and physiological domains. This mechanism is utilized in the medical and physiological fields to develop artificial heart-lung machines and ensure the safe evacuation of hazardous liquids from nuclear power plants, among other applications. The PTT constitutive equation provides accurate estimates of the rheology of various concentrated polymer solutions and melts. These fluid models are widely employed in procedures involving high temperature and heat transfer operations to mimic real fluids. It is now well acknowledged that the majority of biofluids in nature behave as non-Newtonian fluids. Hakeem and Naby [12] employ a Phan-Thien-Tanner fluid model to replicate the complex dynamics of chyme within the small intestine, achieving a strong correlation between their theoretical predictions and experimental results. Recently, many other researchers like Siddiqui et al. [13], Hayat et al. [14, 15], Mahadev and Axita [16], Channakote et al. [17] are also studied the PTT fluid.

The inclusion of porous permeable walls in the analysis of peristaltic flow in planar channels significantly improves the understanding and practical application of these systems in various fields. By incorporating porous permeable walls, researchers can model biological and industrial systems more realistically and explore intricate interactions such as fluid-wall exchange, energy transfer, and stability. This approach enables the development of advanced systems in engineering, medicine, and environmental science. Many researchers have explored the application of generalized Darcy's law in the context of peristaltic flow in porous media. Vajravelu et al. [18] studied peristaltic transport in channels with porous permeable walls. This study builds on their work by incorporating heat transfer and thermal radiation effects within the Phan-Thien-Tanner fluid model in a permeable porous channel. This novel approach provides valuable insights into the thermomechanical interactions of viscoelastic fluids, enhancing our understanding of flow dynamics in complex physiological and industrial settings. Radhakrishnamacharya and Radhakrishnamurty [19] explored the peristaltic mechanism influenced by heat transfer in a porous medium. Channakote and Kalse [20] investigated heat transfer in peristaltic motion of Rabinowitsch fluid in a channel with a permeable wall. Further research on this topic can be found in references [21–29].

The study of bioheat transfer and thermal radiation in peristaltic flow through porous channels is a critical area of research with applications in biomedical engineering and energy systems. Peristaltic flow, characterized by rhythmic wall contractions, is a natural phenomenon in biological systems like blood vessels and the gastrointestinal tract, as well as in industrial processes. Integrating bioheat transfer and thermal radiation provides valuable insights into the thermal and mechanical interactions in these systems. Sunitha and Asha [30] investigated the impact of heat radiation on peristaltic blood flow in a Jeffrey fluid with gold nanoparticles and double diffusion. Kothandapani et al. [31] examined the impact of heat radiation on peristaltic transport in various fluid systems. Rafiq and Abbas [32] studied the effects of heat radiation and viscous dissipation on peristaltic flow of Rabinowitsch viscoelastic fluid in a non-uniform inclined tube. Hayat et al. [33] conducted a detailed analysis of magneto-nanofluid flow in a porous channel, highlighting the significance of radiative peristaltic motion and thermal radiation. Asha and Vijayalaxmi [34] investigated the combined effects of electro-osmosis and Joule heating on peristaltic transport of hyperbolic tangent fluid through a porous medium, particularly in the context of endoscopic applications. Channakote and Siddabasappa [35] explored the heat and mass transfer phenomena in the peristaltic flow of Pan-Thien Tanner liquid, considering wall properties. In a subsequent study, Channakote and Kalse [36] discussed the peristaltic pumping of an Ellis rheological fluid in a non-uniform tube, taking into account convective heat transport and viscous dissipation. Recent research has introduced a comprehensive approach to analyzing peristaltic transport in various flow configurations and geometric variations [37-45].

This research builds on prior studies and seeks to examine the peristaltic flow of a Phan-

Thien-Tanner fluid with heat transfer and thermal radiation through a permeable wall. The investigation aims to understand the interaction between peristaltic motion and heat transfer to enhance flow efficiency. The Phan-Thien-Tanner fluid exhibits distinctive characteristics like shear thickening, shear thinning, and time relaxation. The study analyzes the influence of different parameters on velocity, temperature, pressure rise, and pressure gradient depicted through graphical illustrations.

The physiological and biological fluid studies are motivated by the following key objectives.

- Comprehensive analysis of the impact of heat transfer and thermal radiation on the flow characteristics of the Pan-Thien-Tanner (PTT) fluid model under peristaltic motion.
- Influence of key parameters such as Weissenberg number, permeability, and radiation parameters on flow dynamics.
- Application to biological and industrial peristaltic pumping systems with porous boundaries.
- Examination of the rheological properties of the Pan-Thien-Tanner (PTT) fluid model, capturing its non-linear viscoelastic behavior and relevance to biomedical and industrial applications.
- Novel consideration of peristaltic transport through permeable porous walls, providing insights into fluid dynamics in channels with filtration or absorption.
- Application of the model to systems such as biological peristalsis (e.g., gastrointestinal fluid transport) and porous industrial structures (e.g., filtration devices).
- insight into biomechanical and engineering applications, such as blood flow modeling and industrial transport systems.

2. Constitutive Equations

The extra stress tensor for the linear Phan-Thien and Tanner fluid model is given by Vajravelu et al. [19] and Hayat et al. [15-16].

$$T = -pI + \tau, \tag{1}$$

$$f\big(tr(\tau)\big)\tau + \mathrm{K}\tau^{\nabla} = 2\mu\mathbb{D}, \tag{2}$$

$$\tau^{\nabla} = \frac{d\tau}{dt} - \tau.\mathbb{L}' - \mathbb{L}.\tau, \tag{3}$$

$$f\big(tr(\tau)\big) = 1 + \frac{\epsilon\kappa}{\mu}tr(\tau), \tag{4}$$

where, $\mathbb{L} = \mathrm{grad\,V}$. In the above equations, p represents pressure, I denotes the identity tensor, and μ is the dynamic viscosity. The extra stress tensor is denoted by τ, while $\mathbb{D}$ represents the deformation rate tensor. The relaxation time is given by K, and τ^{∇} corresponds to Oldroyd's upper convected derivative. Furthermore, $\frac{d}{dt}$ signifies the material derivative, tr represents the trace, and a prime indicates the transpose. Notably, when the extensional parameter (ϵ) is set to zero, the PTT model reduces to the upper convicted Maxwell model.

3. Mathematical Formulation

We study the peristaltic flow of an incompressible, non-Newtonian fluid in a planar channel with a permeable wall. A rectangular coordinate system is chosen such that the x-axis lies along the central line of the channel in the direction of wave propagation, while the y-axis is transverse to it. The motion is induced by infinite wave trains with a constant speed c, wavelength λ, and amplitude b, using a fixed rectangular coordinate frame. The physical model is shown in Fig. 1. This study investigates bio-heat transfer and thermal radiation in the peristaltic flow of a viscoelastic fluid. Specifically, we examine the dynamics of peristaltic transport of an incompressible Phan-Thien-Tanner (PTT) fluid model within a planar channel.

The research is conducted under the following assumptions, which also serve as its constraints:

- The shear-dependent properties of the fluid are described using the Phan-Thien - Tanner fluid model.
- Integration of energy equations and radiative heat transfer with the PTT fluid flow, addressing both mechanical and thermal interactions.
- The physical flow problem will be simplified through the application of long-wavelength and low-Reynolds-number approximations.
- Transmitting from an unstable state (laboratory frame) to a stable state (wave frame).
- Heat transfer and thermal radiation are included.
- The study assumes that the region above the permeable wall represents a porous medium, while the region below the wall corresponds to the fluid flow domain.
- Analytical expressions for axial velocity, temperature, pressure gradient, pressure rise, and stream function need to be derived.

The geometry of deforming channel walls is simulated with:

$$h(\bar{x},\bar{t}) = a + b\sin\left(\frac{2\pi}{\lambda}(\bar{X} - c\bar{t})\right), \tag{5}$$

in which a is half width of the channel, b is wave amplitude, λ is wavelength, c is wave speed, $\bar{t}$ is time.

The basic equations of continuity, momentum, temperature, and thermal radiation can be derived following the established standards [15, 16, 19, 41].

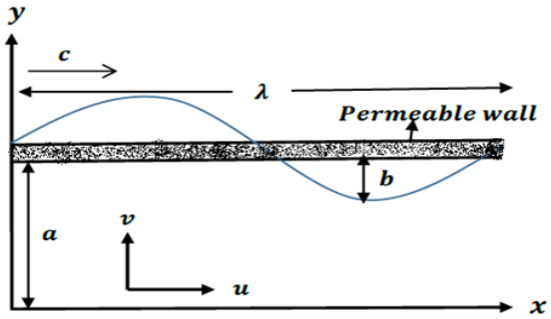

Fig. 1. Flow geometry of the problem

The equations, which can govern the present flow circumstances, Hayat et al. [15] are:

- ***Continuity equation:***

$$\frac{\partial\bar{u}}{\partial\bar{x}} + \frac{\partial\bar{v}}{\partial\bar{y}} = 0, \tag{6}$$

- ***Momentum equation:***

$$\rho\left(\bar{u}\frac{\partial\bar{u}}{\partial\bar{x}} + \bar{v}\frac{\partial\bar{u}}{\partial\bar{y}}\right) = -\frac{\partial\bar{p}}{\partial\bar{x}} + \frac{\partial\bar{\tau}_{xx}}{\partial\bar{x}} + \frac{\partial\bar{\tau}_{xy}}{\partial\bar{y}}, \tag{7}$$

$$\rho\left(\bar{u}\frac{\partial\bar{v}}{\partial\bar{x}} + \bar{v}\frac{\partial\bar{v}}{\partial\bar{y}}\right) = -\frac{\partial\bar{p}}{\partial\bar{y}} + \frac{\partial\bar{\tau}_{yx}}{\partial\bar{x}} + \frac{\partial\bar{\tau}_{yy}}{\partial\bar{y}}, \tag{8}$$

- ***Energy equation:***

$$\rho c_p\left(\bar{u}\frac{\partial\bar{T}}{\partial\bar{x}} + \bar{v}\frac{\partial\bar{T}}{\partial\bar{y}}\right) = k\left(\frac{\partial^2\bar{T}}{\partial\bar{x}^2} + \frac{\partial^2\bar{T}}{\partial\bar{y}^2}\right) + \bar{\tau}_{xx}\frac{\partial\bar{u}}{\partial\bar{x}} + \bar{\tau}_{yy}\frac{\partial\bar{v}}{\partial\bar{y}} + \bar{\tau}_{xy}\left(\frac{\partial\bar{u}}{\partial\bar{y}} + \frac{\partial\bar{v}}{\partial\bar{x}}\right) + \frac{\partial}{\partial\bar{y}}(\bar{q}_r), \tag{9}$$

- ***Fluid equation:***

$$f\bar{\tau}_{xx} + k\left(\bar{u}\frac{\partial\bar{\tau}_{xx}}{\partial\bar{x}} + \bar{v}\frac{\partial\bar{\tau}_{xx}}{\partial\bar{y}} - 2\frac{\partial\bar{u}}{\partial\bar{x}}\bar{\tau}_{xx} - 2\frac{\partial\bar{u}}{\partial\bar{y}}\bar{\tau}_{xy}\right) = 2\mu\frac{\partial\bar{u}}{\partial\bar{x}}, \tag{10}$$

$$f\bar{\tau}_{yy} + k\left(\bar{u}\frac{\partial\bar{\tau}_{yy}}{\partial\bar{x}} + \bar{v}\frac{\partial\bar{\tau}_{yy}}{\partial\bar{y}} - 2\frac{\partial\bar{v}}{\partial\bar{x}}\bar{\tau}_{yx} - 2\frac{\partial\bar{v}}{\partial\bar{y}}\bar{\tau}_{yy}\right) = 2\mu\frac{\partial\bar{u}}{\partial\bar{y}}, \tag{11}$$

$$f\bar{\tau}_{zz} + k\left(\bar{u}\frac{\partial\bar{\tau}_{zz}}{\partial\bar{x}} + \bar{v}\frac{\partial\bar{\tau}_{zz}}{\partial\bar{y}}\right) = 0, \tag{12}$$

$$f\bar{\tau}_{xy} + k\left(\bar{u}\frac{\partial\bar{\tau}_{xy}}{\partial\bar{x}} + \bar{v}\frac{\partial\bar{\tau}_{xy}}{\partial\bar{y}} - \frac{\partial\bar{v}}{\partial\bar{x}}\bar{\tau}_{xx} - \frac{\partial\bar{v}}{\partial\bar{y}}\bar{\tau}_{xy} - \frac{\partial\bar{u}}{\partial\bar{x}}\bar{\tau}_{xy} - \frac{\partial\bar{u}}{\partial\bar{y}}\bar{\tau}_{yy}\right) = \mu\left(\frac{\partial\bar{u}}{\partial\bar{y}} + \frac{\partial\bar{v}}{\partial\bar{x}}\right), \tag{13}$$

$$f = 1 + \frac{\varepsilon k}{\mu}\left(\bar{\tau}_{xx} + \bar{\tau}_{yy} + \bar{\tau}_{zz}\right). \tag{14}$$

Rosseland's approximation is used in radiative heat transfer to describe the radiative heat flux in an optically thick medium. It assumes that radiation behaves diffusively due to multiple scattering and absorption events. The radiative heat flux (q_r) is given by:

$$q_r = \frac{-4\bar{\sigma}}{3\bar{k}}\frac{\partial\bar{T}^4}{\partial\bar{y}} \quad \text{and} \quad q = -k\nabla T \tag{15}$$

here $\bar{\sigma}$ stands for the Stefan-Boltzman constant, $\bar{k}$ is material conductivity, and q is vector of local heat flux. We also supposed that the temperature of the fluid within the flow region is sufficiently small. By expanding T^4 about T_0 and ignoring the higher order term obtained

$$T_0^4 = 4T_0^3T - 3T_0^4 \tag{16}$$

The above appearance and equation (15) now yield.

$$q_r = -\frac{16\sigma\,\bar{T}^3}{3\kappa\mu c}\frac{\partial\bar{T}}{\partial\bar{y}} \tag{17}$$

In above equations, scaling transformations are:

$$\left.\begin{aligned} W_e = \frac{kc}{a}, u = \frac{\bar{u}}{c}, v = \frac{\bar{v}}{c\delta}, x = \frac{\bar{x}}{\lambda}, y = \frac{\bar{y}}{a}, \\ h = \frac{\bar{H}}{a}, \delta = \frac{a}{\lambda}, p = \frac{\bar{p}a^2}{\mu\, c\, \lambda}, \theta = \frac{\bar{T}-\bar{T}_0}{\bar{T}_0} \\ n = \frac{\bar{n}}{n_0}, t = \frac{c\bar{t}}{\lambda}, Pr = \frac{\mu\, c_p}{K}, Ec = \frac{c^2}{c_pT_0}, \\ \phi = \frac{b}{a}, \tau_{ij} = \frac{a\,\tau_{ij}}{c\mu}, R_d = -\frac{16\sigma\,\bar{T}^3}{3\kappa\mu c}, \\ Br = E_cPr,\ E_c = \frac{c^2}{c(T_1-T_0)}, Re = \frac{\rho\, c\, a}{\mu} \end{aligned}\right\} \tag{18}$$

The conditions in (5) can be written as:

$$h = 1 + \phi\,\sin\,(2\pi\,x) \tag{19}$$

We present transformations between fixed and wave frames.

$$\begin{aligned} &\bar{x} = \bar{X} - c\bar{t}, \bar{y} = \bar{Y}, \\ &\bar{u}(\bar{x},\bar{y}) = \bar{U} - c.\ \bar{v}(\bar{x},\bar{y}) = \bar{v} \end{aligned} \tag{20}$$

Saffman boundary conditions play a role in analyzing peristaltic flow, particularly in the study of fluid transport in narrow geometries where slip effects become significant. In the context of peristaltic flow in a planar channel, these boundary conditions modify the conventional no-slip assumption by incorporating a slip length that accounts for the interaction between the fluid and the channel walls.

The appropriate non-dimensional boundary conditions, equations (15, 19, 18), are:

$$\frac{\partial u}{\partial y} = 0, v = 0, at\ y = 0 \tag{21}$$

$$u = -1 - \frac{\sqrt{Da}}{\alpha}\frac{\partial u}{\partial y}, v = -\frac{dv}{dx}, at\ y = h \tag{22}$$

$$\frac{\partial \theta}{\partial y} = 0\ at\ y = 0, \qquad \theta = 1\ at\ y = h. \tag{23}$$

With the help of equation (18) and under the condition of long wavelength and low Reynolds number $\delta \ll 1$ and $Re \approx 0$, equations (6)-(14) takes the following form.

- From momentum equation:

$$\frac{\partial p}{\partial x} = \frac{\partial \tau_{xy}}{\partial x} \tag{24}$$

$$\frac{\partial p}{\partial y} = 0 \tag{25}$$

- From fluid equation:

$$f\tau_{xx} = 2W_e \frac{\partial u}{\partial y}\ \tau_{xy,} \tag{26}$$

$$f\tau_{yy} = 0 = f\ \tau_{zz,} \tag{27}$$

$$f\tau_{xy} = -W_e\ \frac{\partial u}{\partial y}\tau_{yy} + \frac{\partial u}{\partial y}. \tag{28}$$

- From energy equation:

$$(1 + PrRd)\frac{\partial^2 \theta}{\partial y^2} = -Br\tau_{xy}\frac{\partial u}{\partial y}. \tag{29}$$

4. Volume Flow Rate

The dimensional volume flow rate in laboratory frame is inscribed as:

$$Q = \int_0^{\bar{h}} \bar{U}(\bar{X}, \bar{Y}, \bar{t})\, d\bar{Y} \tag{30}$$

where $\bar{h} = \bar{h}(\bar{X}, \bar{t})$, in wave frame the above equation reduces:

$$q = \int_0^{\bar{h}} u(\bar{x}, \bar{y})\, d\bar{y} \tag{31}$$

in which $\bar{h} = \bar{h}(\bar{x})$

From equations (29), (30) and (31) one has:

$$Q = q + c\bar{h}(x) \tag{32}$$

The time averaged over fixed frame $\bar{X}$ is:

$$\bar{Q} = \frac{1}{T}\int_0^T Q\ dt \tag{33}$$

Which after using equation (31) and performing integration leads to:

$$\varphi = F + 1, \tag{34}$$

where,

$$\varphi = \frac{\bar{Q}}{ac}, \quad F = \frac{q}{ac}, \tag{35}$$

$$F = \int_0^h u dy \tag{36}$$

Equation (27) tells that $\tau_{yy} = \tau_{zz} = 0$ and the stress tensors trace changes to τ_{xx}. Integration of equation (24) with $\tau_{xy} = 0\ at\ y = 0$ as the boundary condition (The line of symmetry yields) gives.

$$\tau_{xy} = y\frac{dp}{dx} \tag{37}$$

With help of equation (26) and (27), we can write:

$$\tau_{xx} = 2\epsilon W_e \tau_{xy}^3 \tag{38}$$

From equations(14), (26) and (38), we get:

$$\frac{\partial u}{\partial y} = \tau_{xy} + 2\epsilon W_e^2 \tau_{xy}^3 \tag{39}$$

Substituting equation (38) in to (39), we obtain.

$$\frac{\partial u}{\partial y} = y\frac{dp}{dx} + 2\epsilon W_e^2 \left(y\frac{dp}{dx}\right)^3 \tag{40}$$

5. Analytical Solution

Utilizing the boundary conditions defined in equations (21) and (22) to address equation (40), we obtain:

$$\begin{aligned} u = &-1 - \frac{(y^2 - h^2)}{2}\left(\frac{dp}{dx}\right) \\ &+ \frac{2\epsilon W_e (y^4 - h^4)}{4}\left(\frac{dp}{dx}\right)^3 \\ &- \frac{\sqrt{Da}}{\alpha}\left[\left(\frac{dp}{dx}\right)h + 2\epsilon W_e \left(\frac{dp}{dx}\right)^3 h^3\right], \end{aligned} \tag{41}$$

Making use of equation (41) into equation (36), we attain at:

$$6W_e \in h^5\left(\frac{dp}{dx}\right)^3 + 5h^3\left(\frac{dp}{dx}\right) + 15(F+h) + \frac{\sqrt{\mathrm{Da}}}{\alpha}\left(h^2\frac{dp}{dx} + 2h^4 W_e \in \left(\frac{dp}{dx}\right)^3\right) = 0 \quad (42)$$

As Da approaches zero the equation (41-42) corresponds to the velocity and pressure expressions presented by Hayat et al. [15].

Due to nonlinearity, it is difficult to arrive at the analytical solution to equation (42). As a result, the solution is obtained using the standard perturbation approach. We expand $\frac{dp}{dx}$ in terms of the parameter ($|W_e| \ll 1$) in order to use the perturbation approach as follows:

$$\frac{dp}{dx} = \left(\frac{dp}{dx}\right)_0 + W_e\left(\frac{dp}{dx}\right)_1 \quad (43)$$

The solution of equation (42) with the help of equation (43) is given by:

$$\frac{dp}{dx} = -\frac{3(F+h)\alpha}{h^2\left(3\sqrt{\mathrm{Da}}+h\alpha\right)} - \frac{6h^2\left(-\frac{135\sqrt{\mathrm{Da}}(F+h)^3\alpha^3\epsilon}{h^6\left(3\sqrt{\mathrm{Da}}+h\alpha\right)^3} - \frac{27(F+h)^3\alpha^4\epsilon}{h^5\left(3\sqrt{\mathrm{Da}}+h\alpha\right)^3}\right)W_e}{5\left(3\sqrt{\mathrm{Da}}+h\alpha\right)}. \quad (44)$$

By solving equation (29) with boundary condition (23), the expression for temperature is given as:

$$\theta = 1 + \frac{5\mathrm{Br}\left(\frac{dp}{dx}\right)^2(h^4-y^4) + 4\mathrm{Br}\left(\frac{dp}{dx}\right)^4 W_e(h^6-y^6)\epsilon}{60(1+\mathrm{Pr\,Rd})} \quad (45)$$

The pressure difference across the one wavelength is calculated from the previous equation:

$$\Delta p = \int_0^1 \frac{\partial p}{\partial x}dx. \quad (46)$$

$$F_\lambda = \int_0^1 h\left(-\frac{\partial p}{\partial x}\right)dx. \quad (47)$$

6. Results and Discussion

In this section, the exact solutions that were calculated in the prior sector are now visually exhibited, allowing us to scrutinize the belongings of several (dimensionless) significant constraints on the flow profile, with W_e (Weissenberg number), ϵ (PTT parameter), Da (Darcy number), α (slip parameter), Rd (Thermal radiation parameter) and Pr (Prandtl number) (i.e., temperature profile, velocity profile, pressure gradient, pressure rise). The graphical plots illustrate the accuracy of the mathematical solutions, enabling a thorough analysis of the results. The velocity and temperature profiles shown in the graphs confirm that the boundary conditions in our case were maintained. The calculated mathematical solutions successfully satisfy the equations and boundary conditions. It is widely recognized that the axial velocity profiles display a parabolic shape, typical of slip flow, with zero velocity at the walls and maximum velocity at the channel center.

6.1. Flow Characteristics

Figures 2(a)-(c) illustrate the impact of physical factors on the material characteristics of regulating fluid flow.

In Figure 2(a), the velocity profile behavior is demonstrated with varying Darcy numbers (Da), showing a gradual decrease in axial flow velocity as Da increases. A higher porosity parameter corresponds to lower permeability, resulting in a reduced gap for fluid flow and leading to a decrease in velocity. Therefore, a porous medium acts as a resistive force that impedes fluid velocity.

Figure 2(b) shows how the slip parameter, α, affects the velocity distribution along the $x-axis$. The slip parameter α, quantifies the degree to which the boundary allows fluid movement, representing the amount of "slip" occurring at the surface. An increase in α indicates a decrease in frictional resistance at the boundary, resulting in reduced drag on the fluid as it flows along the surface. This allows the fluid to gain more momentum, leading to a higher velocity profile. As a result, the fluid can move more freely near the wall, enhancing the transfer of momentum and improving efficiency.

The impact of the Weissenberg number (W_e) is depicted in Fig. 2(c). It is evident from the figure that the Weissenberg number (W_e) decreases the velocity of the liquid. The Weissenberg number (W_e) represents the ratio of elastic to viscous forces in the fluid. As the Weissenberg number (W_e) increases, the fluid's elastic behavior becomes more dominant, indicating that the fluid can store more elastic energy rather than converting it into kinetic energy.

This increased elastic effect opposes the fluid's motion, leading to a reduction in velocity. Essentially, as the Weissenberg number (W_e) increases, the fluid exhibits more elastic characteristics, which dampen the flow and result in a lower speed along the x-direction.

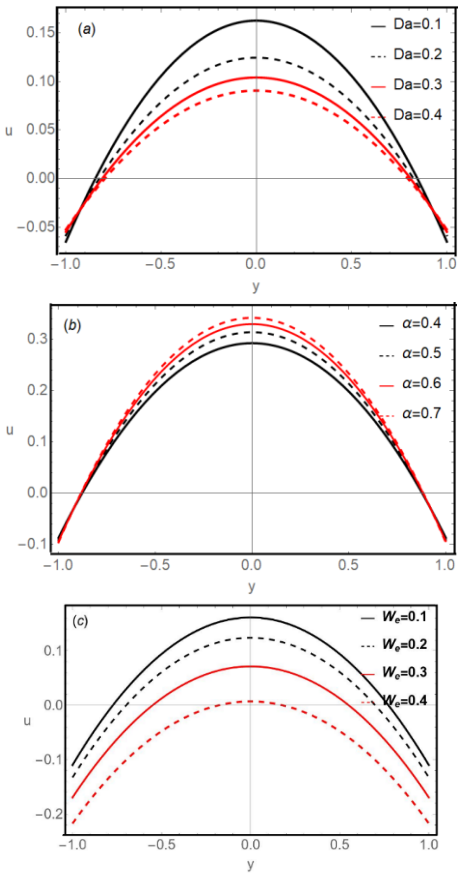

Fig. 2. Velocity distribution for diverse values of a) Da, b) α, c) W_e through $\varphi = 0.95, \phi = 0.6, \varepsilon = 0.1, x = 0.25$

6.2. Heat Characteristics

In this sub part, the impacts of several influential parameter through the temperature field are discussed since it has comprehensive series of applications in manufacturing and mediational procedure. Hence the graphs of the temperature field for diverse values of W_e, Brinkmann number Br, Darcy number Da, Prandtl number Pr, and thermal radiation Rd are displayed in Figs. 3(a)-(e) respectively. Figure 3(a) shows the impact of varying the Weissenberg number (W_e) on the liquid's temperature. The Weissenberg number is a dimensionless parameter that compares elastic effects to viscous forces in a fluid. A higher Weissenberg number indicates stronger elastic behavior, allowing the fluid to store and release energy during deformation. This reduces heat generation by converting some mechanical energy into elastic energy. This property is beneficial in practical applications such as polymer processing and lubrication systems. By controlling the Weissenberg number, temperature can be regulated, viscosity optimized, energy efficiency improved, and lubricant lifespan extended. Manipulating the Weissenberg number is essential for optimizing thermal management in industrial processes. Figure 3(b) demonstrates the effect of the Brinkmann number (Br) on the fluid temperature. Physically, Br represents the ratio of viscous heating where mechanical energy is converted into thermal energy through friction to the rate of heat conduction away from the fluid. As Br increases, the viscous dissipation becomes more pronounced relative to the fluid's ability to remove heat, leading to a rise in the temperature. This is particularly significant in practical applications such as lubrication systems or polymer processing, where managing viscous heating is essential to prevent overheating, maintain material integrity, and optimize process efficiency. Figures 3(c)-(e) illustrate the temperature distribution for varying Darcy number (Da), Prandtl number (Pr), and thermal radiation parameter (Rd). Increasing Da, Pr, and Rd leads to a reduction in the temperature profile. A higher Da signifies greater permeability, which enhances fluid motion, convective heat transfer, and cooling efficiency, resulting in lower fluid temperatures. Higher Pr leads to a thinner thermal boundary layer, a steeper temperature gradient, and lower surface temperatures see (3d). An increase in Rd causes more radiative heat loss, further decreasing the temperature. Together, these parameters improve fluid flow, sharpen the thermal gradient, and increase radiative heat dissipation, leading to a lower temperature distribution. Da represents the permeability of the porous medium, with higher values promoting better fluid flow and heat dissipation, thus reducing the temperature. Pr quantifies the ratio of momentum to thermal diffusivity, where a higher Pr indicates faster momentum diffusion, resulting in lower temperatures. Rd measures thermal radiation effects, with larger values increasing radiative heat loss and lowering the overall temperature. In peristaltic transport with a permeable boundary, these factors collectively enhance heat removal, promoting a cooler PTT fluid temperature profile.

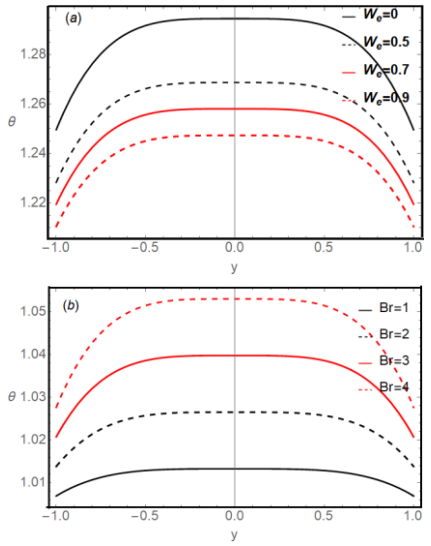

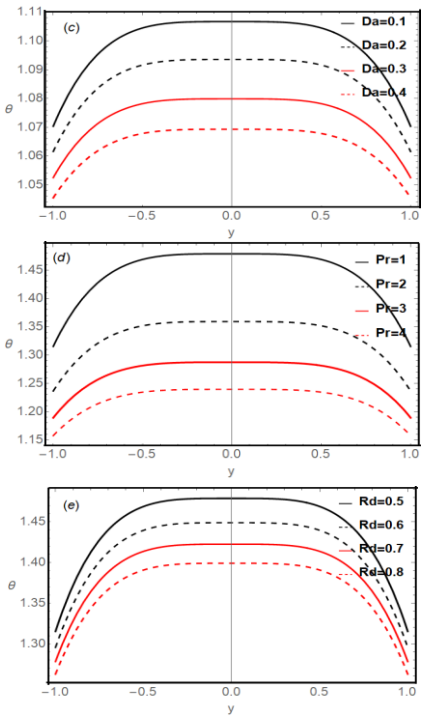

Fig. 3. Temperature distribution for diverse a) W_e, b) Br, c) Da, d) Pr, e) Rd through $\varphi = 0.95, \phi = 0.6, \varepsilon = 0.1, x = 0.25$

6.3. Pressure Gradient

The axial pressure gradient profiles, or the pressure gradient vs the axial coordinate along the channel's center line in one period with fixed time and flow rate, are shown in Figs. 4(a)-3(c). Due to the nature of the peristaltic flow, it is evident that the pressure gradient profiles are uniform and display periodicity; specifically, they are minimal at fully relaxed wall sites and exhibit highest values at fully contracted wall sites. Figure 4(a) illustrates how the Weissenberg number (W_e) which quantifies the ratio of elastic to viscous forces in the fluid-e and affects the pressure gradient across the channel. As Weissenberg number (W_e) increases, the elastic forces become more prominent, leading to a steeper pressure gradient. Specifically, in the regions near the channel walls ($x \in [0, 0.5]$ and $[1, 1.4]$), the pressure changes only gradually, suggesting that the boundary layers experience relatively mild elastic effects. However, in the central region ($x \in [0.6, 0.9]$), the pressure gradient is much more pronounced, indicating that the influence of a higher W_e, which may represent additional rheological properties such as fluid relaxation, intensifies the elastic stresses in this core area. In addition, Figure 4(b) shows that for a fixed thermal parameter (Θ), increasing the Darcy number (Da) results in a lower overall pressure. Physically, a larger Da implies a more permeable porous medium, which facilitates easier fluid flow and reduces the pressure required to drive the motion through the channel. Together, these observations highlight the complex interplay between fluid elasticity, structural properties, and the permeability of the medium, all of which critically influence the pressure distribution in the system. In Figure 4(c), it is observed that as the slip parameter α increases, the pressure gradient also increases.

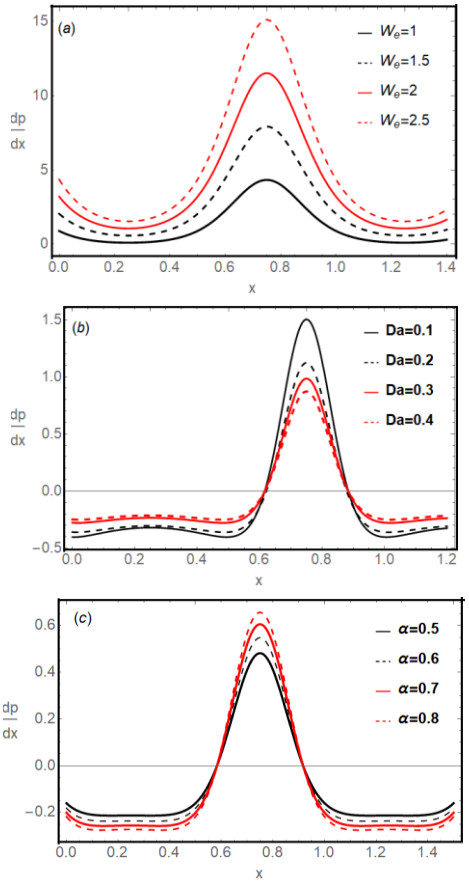

Fig. 4. Pressure gradient for diverse a) W_e, b) Da, c) α through $\varphi = 0.95, \phi = 0.6, \varepsilon = 0.1$

6.4. Pumping Characteristics

The well-known phenomenon of peristaltic transport is associated with mechanical pumping. Therefore, it is important to investigate the pumping performance based on existing studies. This pumping method enables the controlled transfer of liquid volume from one area to another without any disturbance. The graphs depict the pressure rise for various values of the Weissenberg number (W_e), slip parameter (α), and Darcy number (Da). Figures 5(a)-5(c) illustrate the change in pressure rise (Δp) with respect to the flow rate (Q). A linear relationship between flow rate and pressure is observed, with three distinct pumping regions: (i) pumping region ($\Delta p > 0$), (ii) free pumping region ($\Delta p = 0$), and (iii) augmented pumping region ($\Delta p < 0$). The influence of the Weissenberg number (W_e) on pressure increase is shown in Figure 5(a). The Weissenberg number is a dimensionless quantity

that measures the ratio of elastic to viscous forces in the fluid. Its effect on the pumping performance is twofold: In the pumping region, an increase in W_e results in a decrease in the pressure rise. This suggests that as the elastic effects of the fluid become more pronounced, they tend to oppose the pressure buildup, possibly by allowing the fluid to stretch and relax more easily. Conversely, in the augmented pumping region, a higher W_e leads to a more pronounced negative pressure, thereby enhancing the pumping effect. This indicates that under conditions where the system benefits from a negative pressure gradient, the elastic properties actually help to drive the fluid more efficiently. Previous studies by Hayat et al [15], support this observation, particularly for linear PTT fluids. From Figure 5 (b), it is seen that the rise in pressure is an increasing function of slip parameter α in pumping region where as it is decreasing function in augmented pumping region. The impact of Darcy number (Da)on pressure rise is illustrated in Figure 5(c). The Darcy number characterizes the permeability of the medium through which the fluid flows. Its impact on the pressure rise is found to be similar to that of the Weissenberg number.

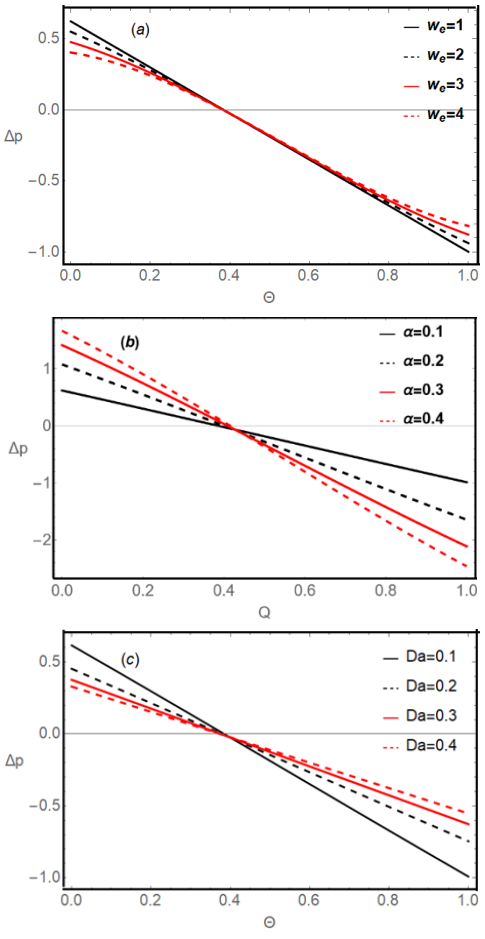

Fig. 5. Variations of pressure gradient Δp versus Q for a) W_e, b) α, c) Da through $\varphi = 0.95, \phi = 0.6, \varepsilon = 0.1$.

6.5. Validition

The results obtained by the developed code are validated with the results presented by channakote et al. [17] as the limiting case, i.e. $Da = 0$ (See Table 1 and Figure 6).

Table 1. Results of validation

Channakote et al. [17] $U_{hs} = 0$			
$w_e = 0{,}1$	$w_e = 0{,}2$	$w_e = 0{,}3$	$w_e = 0{,}4$
0,3602	0,1867	−0,03191	−0,2665
0,2195	0,06742	−0,1292	−0,3416
−0,2182	−0,3093	−0,4366	−0,5764
−1	−1	−1	−1
Present work $Da = 0$			
$w_e = 0{,}1$	$w_e = 0{,}2$	$w_e = 0{,}3$	$w_e = 0{,}4$
0,3603	0,18674	−0,0321	−0,2765
0,2196	0,0675	−0,1310	−0,3426
−0,2183	−0,30946	−0,4470	−0,5864
−1	−1	−1	−1

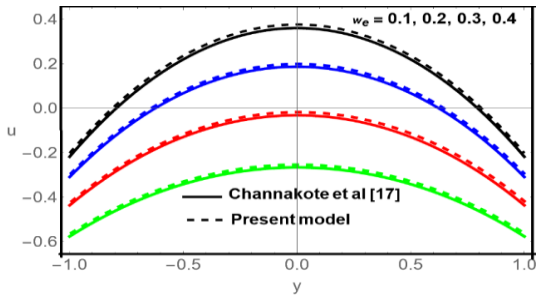

Fig. 6. Comparision of the computational velocity with channakote at al.[17] for different values of w_e when $\phi = 0.5, \epsilon = 0.3, x = 0.25, \varphi = 0.95$.

7. Conclusions

In this research, a mathematical analysis has been performed on peristaltic flow caused by heat and thermal radiation in viscous movement through a permeable channel. The primary aim of this research is to emphasize the impacts of thermal radiation, permeable boundaries, and Phan-Thien-Tanner fluid model characteristics on velocity, temperature, pressure gradient, and pressure rise occurrences.

The key results of this study are outlined as follows:

- Velocity is decreasing function for W_e and Da whereas it is an increasing function of slip parameter.
- The temperature enhances with increasing values of W_e and Br.
- The pressure gradient increases with increasing Weissenberg number W_e and slip parameter α.
- Pressure gradient reduces with increasing permeability (higher Darcy number).

- Pressure rise reduces with increasing permeability (higher Darcy number) and Weissenberg number, in the pumping region whereas the reverse trend is observed in the augmented pumping region.

The findings have important real-world applications, ranging from biomedical devices such as artificial peristaltic pumps used in drug delivery systems and minimally invasive surgical procedures to industrial processes involving the handling of complex fluids, such as polymer processing, oil recovery in porous media, and the design of microfluidic cooling systems. These insights pave the way for improved design and control of systems where precise fluid transport and thermal management are critical. Moreover, developing realistic geometrical models that account for the irregular and varying cross-sections of biological tissues would enhance the practical relevance of the findings. Exploring different boundary conditions that represent various biological interfaces could also provide a more detailed understanding of the system's behaviors under diverse physiological conditions. Future research could also focus on experimental validation and examine the effects of varying electric field strengths and nanofluids.

Nomenclature

a	Radius of the tube
b	Wave amplitude
Br	Brinkmann number
c	Wave speed
Da	Darcy number
I	Identity tensor
k	Relaxation time
Pr	Prandtl number
Re	Reynolds number
t	Time
T	Cauchy stress tensor
tr	Trace
(u, v)	Velocity components (in moving frame)
$(\overline{\mathrm{U}}, \overline{\mathrm{V}},)$	Velocity components (in laboratory frame)
$\mathrm{W_e}$	Weissenberg number
$(\overline{\mathrm{X}}, \overline{\mathrm{Y}})$	Axes are taken respectively parallel and transverse to the direction of wave propagation
$\mathbb{D}$	Deformation-rate tensor
δ	Wave number
ϕ	Phase difference varying in the range $0 \leq \phi \leq \pi$
λ	Wavelength

Funding Statement

This research did not receive any specific grant from funding agencies in the public, commercial, or not-for-profit sectors.

Conflicts of Interest

The author declares that there is no conflict of interest regarding the publication of this article.

Authors Contribution Statement

Ballekere Ramakrishna Mahalakshmi: Writing – Original Draft; Investigation; Methodology; Visualization.

Mahadev Madivalappa Channakote: Writing - Review, Project administration; Resources; Software; Supervision.

Shekar Marudappa: Validation, Writing – Review & Editing, Proofread etc.

Shivakumar Biradar: Writing – Review & Editing, etc.

References

[1] Latham, T.W., 1966., *Fluid motions in peristaltic pump.* (Doctoral dissertation, Massachusetts Institute of Technology).

[2] Shapiro A., Jaffrin M., & Weinberg H., 1969. Peristaltic pumping with long wavelength at low Reynolds number. *Journal of Fluid Mechanics*, 35, pp. 799-825.

[3] Hayat T., Farooq S., Ahmed B., & Alsaedi A., 2016. Characteristics of Convective heat transfer in the MHD peristalsis of Carreau fluid with Joule heating. *AIP Advances*, 6, 045302.

[4] Akbar N., Nadeem S., & Khan, Z., 2014. Numerical simulation of peristaltic flow of a Carreau nanofluid in a asymmetric channel. *Alexandria Engineering Journal*, 53, pp. 191-197.

[5] Rathod, V. P., & Mahadev, M., 2012. Peristaltic flow of Jeffrey fluid with slip effect in an inclined channel. *Journal of Chemical Biological Physics*, 2, pp. 1987–1997.

[6] Rathod, V. P., & Channakote, M. M., 2011. A study of ureteral peristalsis in a cylindrical tube through a porous medium. *Advances in Applied Science and Research*, 3, pp. 134–140.

[7] Srinivas, A.N.S., & Hemadri Reddy, R., 2014. Peristaltic transport of a casson fluid in a channel with permeable walls. *International Journal of Pure and Applied Mathematics*, 90 (1), pp. 11-24.

[8] Vajravelu, K., Sreenadh, S., Hemadri Reddy, R., & Murugesan, K., 2009. Peristaltic transport of a casson fluid in contact with Newtonian fluid in a circular tube with permeable wall. *International Journal of Fluid Mechanics Research*, 36(3), pp. 244-254.

[9] Akhtar, S., Luthais McCash, B., Nadeem, S., Saleem, S. & Issakhov, A., 2009. Mechanics of non-Newtonian blood flow in an artery having multiple stenosis and electroosmotic effects. *Science Programme*, 104, pp. 1-15.

[10] Prakash, G., Pranab Kumar M., Anubhab, D., & Suman, C., 2016. Entropy generation minimization in an electroosmotic flow of non-Newtonian fluid: effect of conjugate heat transfer. *ASME Journal of Heat Transfer*, 138(5), 051704.

[11] Haroon, T., Ansari, A. R., Imran, A., Siddiqui, A. M., 2012. On the ciliary transport of an axisymmetric power law fluid through a tube. *Mathematics in Engineering, Science and Aerospace,* 3(2), pp. 131-142.

[12] Abd El Hakeem, & Abd El Naby, 2009. Creeping flow of Phan-Thien–Tanner fluids in a peristaltic tube with an infinite long wavelength. *Journal of Applied Mechanics,* 76, 064504-1.

[13] Siddiqui, A.M., Azim, Q. A., Ashraf, A., & Ghori, Q. K., 2009. Exact solution for peristaltic flow of PTT fluid in an inclined planar channel and axisymmetric tube. *International Journal of Nonlinear Sciences and Numerical Simulation,* 10, pp. 75-92.

[14] Hayat, T., Noreen, S., Ali, N., & Abbasbandy, S., 2012. Peristaltic motion of Pan-Thien-Tanner fluid in a planar channel. *Numerical methods for Partial Differential Equations*, 28, pp. 737-748.

[15] Hayat, T., Noreen, S., & Ali, Nasir., 2010. Effect of an induced magnetic field on the peristaltic motion of Phan-Thien-Tanner fluid. *Zeitschriftfür Naturforschung A,* 65(8), pp. 665-676. https://doi.org/10.1515/zna-2010-8-907

[16] Mahadev, M., & Axita Mohanta, 2023. Thermal radiation effect on Pan-Thien-Tanner liquid model obeying peristaltic activity with cilia waves. *World Scientific News*, 183, pp. 210-226.

[17] Channakote, M.M., Shekar, M., & Dilipkumar, V.K., 2024. Electro-osmotic effect on peristaltic flow of Phan–Thien–Tanner fluid in a planar channel. *The Anziam journal*, 66, pp. 1-21.

[18] Vajravelu, K., Sreenadh, S., Lakshminarayana, P., Sucharitha, G., & Rashidi, M.M., 2015. Peristaltic flow of Phan-Thien-Tanner fluid in an asymmetric channel with porous medium. *Journal of Applied Fluid Mechanics*, 9, pp. 1615-1625.

[19] Radhakrishnamacharya, G., & Radhakrishnamurty, V., 2007. Peristaltic flow and heat transfer in a vertical porous medium. *Applied Mathematics and Computer*, 153, pp. 763-777.

[20] Channakote, M., M., & Kalse, D.V., 2021. Heat transfer in peristaltic motion of Rabinowitsch fluid in a channel with permeable wall. Applications and Applied Mathematics: An International Journal, 16(1), pp. 1-19.

[21] Vajravelu K., Radhakrishnamacharya, G., & Radhakrishnamurty V., 2007. Peristaltic flow and heat transfer in a vertical porous annulus with long wave approximation. Int. J. Nonlinear Mech., 42(5), pp. 754–759.

[22] Madiha Takreem, K., Venkateswarlu, B., Misra, A., Satya Narayana, P.V. and Harish Babu, D., 2025. Optimization of heat transfer characteristics of Casson hybrid nanofluid flow over a porous exponentially elongating surface using RSM approach. *Journal of Thermal Analysis and Calorimetry,* 150(3), pp. 2133-2149. https://doi.org/10.1007/s10973-024-13840-y

[23] Babu, D.H., Naidu, K.K., Babu, B.H., Raju, K.V., Reddy, S.H. and Narayana, P.S., 2024. Numerical and neural network approaches to heat transfer flow in MHD dissipative ternary fluid through Darcy-Forchheimer permeable channel. *Case Studies in Thermal Engineering*, 60, p.104777.

[24] Mekheimer, Kh. S., & Abd Elmaboud, Y., 2008. Peristaltic flow through a porous medium in an annulus: Application of an endoscope. *Applied Mathematics & Information Sciences*, 2, pp. 103-121.

[25] Srinivas, S., & Gayathri, R., 2009, Peristaltic transport of a Newtonian fluid in a vertical asymmetric channel with heat transfer and porous medium. *Applied Mathematics Computer*, 215, pp. 1855-1960.

[26] Akbar, N.S., & Butt, A.W., 2018. Ferromagnetic nano model study for the

peristaltic flow in a plumb duct with permeable walls. *Microsyst Technol*, 25(4), pp. 1227–1234.

[27] Anas A.M., Arafa, Sameh E., & Ahmed, Allan, M.M., 2022. Peristaltic flow of non-homogeneous nanofluids through variable porosity and heat generating porous media with viscous dissipation: Entropy analyses. *Case Studies in Thermal Engineering*, 32, 101882.

[28] Maimona Rafiq, Asma Shaheen, Youssef Trabelsi, Sayed M. Eldin, M. Ijaz Khan & Dhia Kadhm Suker, 2023. Impact of activation energy and variable properties on peristaltic flow through porous wall channel. *Science Report*, 13, 3219.

[29] Eldabe, N.T.M., Shaker, M.O., & Maha, S.A., 2018. Peristaltic flow of MHD Jeffrey fluid through porous medium in a vertical channel with heat and mass transfer with radiation. *Journal of Nanofluid*,7, pp. 595–602.

[30] Sunitha, G., & Asha, S.K., 2019. Influence of thermal radiation on peristaltic blood flow of a Jeffrey fluid with double diffusion in the presence of gold nanoparticles. *Inf. in Med. Unl.* 17, pp. 1-13.

[31] Kothandapani, M., & Prakash, J., 2015. Effects of thermal radiation parameter and magnetic field on the peristaltic motion of Williamson Nano fluids in a tapered asymmetric channel, Indian Institute of Technology. *Journal of Heat and Mass Transfer*, 81, pp. 234-245.

[32] Rafiq, M.Y, & Abbas, Z., 2021. Impacts of viscous dissipation and thermal radiation on Rabinowitsch fluid model obeying peristaltic mechanism with wall properties. Arab. *Journal of Science and Engineering*, 12, 05870-7.

[33] Hayat, T., Saima Rani, Alsaedi, A., & Rafiq, M., 2017. Radiative peristaltic flow of magneto nanofluid in a porous channel with thermal radiation. *Results in Physics*, 7, pp. 3396-3407.

[34] Kotnurkar, A.S., & Talawar, V.T., 2022. Impact of electro osmosis and joule heating effects on peristaltic transport with thermal radiation of hyperbolic tangent fluid through a porous media in an endoscope. *Partial Differential Equations in Applied Mathematics*, 5, 100340.

[35] Channakote, M.M., & Siddabasappa, C., 2024. Heat and mass transfer analysis on peristaltic transport of PTT fluid with wall properties. *Latin American Applied Research*, 54, pp. 1-9.

[36] Channakote, M. M., & Kalse, V. D., 2022. Combined convective and viscous dissipation effects on peristaltic flow of Ellis fluid in non uniform tube. *Journal of Naval Architecture and Marine Engineering*, 19, pp. 1-12.

[37] Adil Wahid, B., Akbar, N.S., & Mir, N.A., 2020. Heat transfer analysis of peristaltic flow of a Phan-Thien-Tanner fluid model due to metachronal wave of cilia. *Biomechanics and modelling in mechanobiology*, 19(5), pp. 1925-1933.

[38] Hussain, S., Ali, N., & Ullah, K., 1977. Peristaltic flow of Phan-Thien-Tanner fluid: effects of peripheral layer and electroosmotic force. *Rheological Acta*, 58, pp. 603-618.

[39] Naveed Imran, Maryiam Javed, Muhammad Sohail, and Iskander Tlili, 2020. Simultaneous effects of heterogeneous-homogeneous reactions in peristaltic flow comprising thermal radiation: Rabinowitsch fluid model. *Journal of Materials Research and Technology*, 9(3), pp. 3520-3529.

[40] Noreen, S., 2017. Pressure driven flow of PTT fluid in a channel with heat transfer and inclined magnetic field. International. *Journal of Applied Computer and Mathematics*, 3, pp. 497–1509.

[41] Asha, S.K., & Sunitha, G., 2020. Thermal radiation and hall effects on peristaltic blood flow with double diffusion in the presence of nanoparticles. *Case Studies in Thermal Engineering*, 17, 100560.

[42] Rosen, J.B., 1961. The gradient projection method for nonlinear programming: Part II nonlinear constraints. *Journal of the Society for Industrial and Applied Mathematics*, 9(4), pp. 514-532.

[43] Mahadev M C., & Shekar M., 2024. Peristalsis of electro-osmotic Jeffrey fluid in the presence of thermal radiation and heat transfer with the permeable wall. *Jordan Journal of Mathematics and Statistics*, 17(3), pp. 401-412.

[44] Karunakaran V., & Renganathan T., 2023. A Review on solution techniques and application of peristaltic transport in generalized newtonian fluid. *Journal of Heat and Mass Transfer Research*, 10(20), pp. 223-244.

[45] Nilam, V., Suresh M, X., Dondu, H.B. and Avula, B.B., 2024. Comprehensive analysis of normal shock wave propagation in turbulent non-ideal gas flows with analytical and neural network methods. *Physics of Fluids*, 36(9).